Available online at www.sciencedirect.com
SCIENCE DIRECT®
Tunnelling and Underground Space Technology 21 (2006) 56–67
Tunnelling and Underground Space Technology incorporating Trenchless Technology Research
www.elsevier.com/locate/tust

Excavation of a cavern for high-pressure storage of natural gas

R. Glamheden *, P. Curtis

FB Engineering AB, Södra Förstadsgatan 26, SE-211 43 Malmö, Sweden

Received 3 April 2004; received in revised form 15 June 2005; accepted 15 June 2005
Available online 24 August 2005

Abstract

During the last 20 years a new storage technology has been under development for the world market. The first lined rock cavern (LRC) for storage of gas under high-pressure, constructed at Skallen, in southwest Sweden is now complete. The project is a joint venture between Sydkraft of Sweden and Gaz de France for the development and demonstration of the LRC-Technology. The excavation work was completed at the end of 2000 and the construction work was finished 2002. After a test period of one and a half years, the facility has been in commercial operation as a part of the Swedish gas grid since early 2004. The main features of the below ground facility are a 1 km long access tunnel, a 115 m deep vertical shaft and a 40,000 m^3 rock cavern. The cavern is designed as a silo, 52 m high and 36 m in diameter, with a large cupola and curved form bottom. The host rock in the area is crystalline gneiss of good quality, intersected by amphibolite dikes of poor quality. During construction, the stability of the cavern has been monitored by extensometers around the cavern and convergence measurements in the cupola. Only small deformations of a few millimeters have been recorded. This paper describes the cavern rock design and the experiences from the excavation works, along with a comparison of predicted and recorded deformations. A number of rock mechanic analyses have been carried out to determine rock stability and rock support.

Keywords: Crystalline rock; Underground gas storage; Cavern excavation; Rock deformation; Rock support

1. Introduction

The LRC concept has been developed in Sweden since mid 1980s by Sydkraft as the coordinator. The first LRC storage of industrial scale, the LRC Demo plant, was designed and built by two major European energy companies:

- Gaz de France, one of the world's principal gas operators.
- The Sydkraft Group, the second largest combined electricity and gas utility in Sweden.

The project is partially financed by the European Union's Thermie research and development program.

The obvious purpose of a storage is to balance the supply of natural gas with the variations in consumption within an area, like seasonal fluctuations, short term adjustment (weekly and daily), and peak winter demand. There are also other purposes that a storage can fulfil like, e.g., strategic role with security of delivery and possibilities to buy and sell gas.

The storage design involves the gas being stored in a steel and concrete lined rock cavern under high-pressure. The steel lining ensures gas tightness whilst the main load is transferred via the lining to the surrounding supporting rock mass. Lined rock cavern storage is competitive with conventional LPG/LNG facilities with the additional benefit of allowing the working gas to be cycled many times a year. The LRC storage facilities also presents several innovative aspects that will play a

* Corresponding author. Tel.: +46 040 660 25 51; fax: +46 040 660 25 99.
E-mail address: rune.glamheden@fbe.se (R. Glamheden).

0886-7798/$ - see front matter © 2005 Elsevier Ltd. All rights reserved.
doi:10.1016/j.tust.2005.06.002

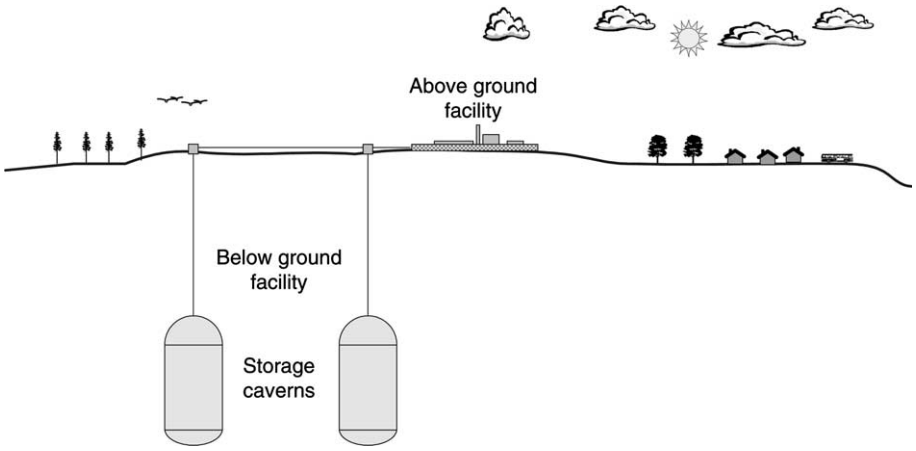

Fig. 1. Schematic illustration of an LRC gas storage plant (after Johansson, 2003).

major role for the implementation of the storage concept to the gas industry. Some are listed below:

- high degree of flexibility since there is a wide range of possible siting due to geological requirements;
- high deliverability due to structural stability of the cavern;
- low environmental impact;
- structurally stable storage which implies possibilities to operate the LRC to a low pressure.

A commercial facility would consist of multiple caverns, laid out according to local site conditions and storage capacity requirements. Each cavern having a vertical cylindrical shape with a diameter of approximately 40–45 m and a height of approximately 100–120 m. The top of the cavern is located at a depth of 100–150 m. A schematic illustration of an LRC gas storage plant is presented in Fig. 1.

The cavern construction process is relatively straightforward, employing top-level conventional mining techniques. The first step is the excavation of the access tunnels and then the excavation of the individual caverns. Upon completion of the caverns, a shaft with piping connects each cavern to the surface facilities.

The LRC storage concept has already been tested in a pilot project in Grängesberg, Sweden. The cavern successfully withstood a pressure of over 50 MPa. The construction of the LRC Demo Plant at Skallen was completed in June 2002. Commercial operation of the LRC Demo Plant began in 2004.

2. Site description

The plant consists of a surface facility, a 40,000 m^3 underground cavern and a 3.2 km long pipeline for connection to the gas grid. The facility is a demonstration plant and the 40,000 m^3 volume represents about a third to quarter of the size of a commercial cavern. The surface facility houses the mechanical parts used for operation and includes coolers, heaters and compressors, along with supervisory and control equipment. These facilities are located at the top of a hill.

2.1. Layout and geometry

The shape of the storage cavern is a vertical cylinder with a spherical top and rounded saucer-like bottom. The diameter is 36 m and the height 52 m. The top of the cavern is at a depth of 115 m below the ground surface. The cavern shape was primarily chosen to obtain a uniform strain distribution in the lining during pressurization. However, the cupola geometry also has advantages for the cavern stability.

The access tunnel to the rock cavern has a cross-sectional area of 28 m^2 and slopes downwards at a gradient of 1:7. It consists of four main sections: an approach tunnel; a tunnel above the cavern for access to the shaft; a lower cavern tunnel at the base of the cylinder; and an upper cavern tunnel at the base of the spherical dome. A 1 m diameter, 90 m long, shaft links the gas storage cavern with the surface facility, see Fig. 2.

2.2. Geology and rock mass quality

The rock mass in the project area is dominated by a gray to reddish-gray gneiss. Generally, the gneiss is of good quality with a low fracture frequency. Surface outcrops show a frequency of less than one joint per meter and RQD values from the drill cores were generally high, over 80%. The seismic refraction profiling gave velocities of 5100–5300 m/s. Overall these pre-construction values correlated well with what was actually encountered during the excavation work.

The gneiss is intersected by planar zones of poor quality rock with a higher fracture frequency. These zones are associated with dykes of amphibolite with

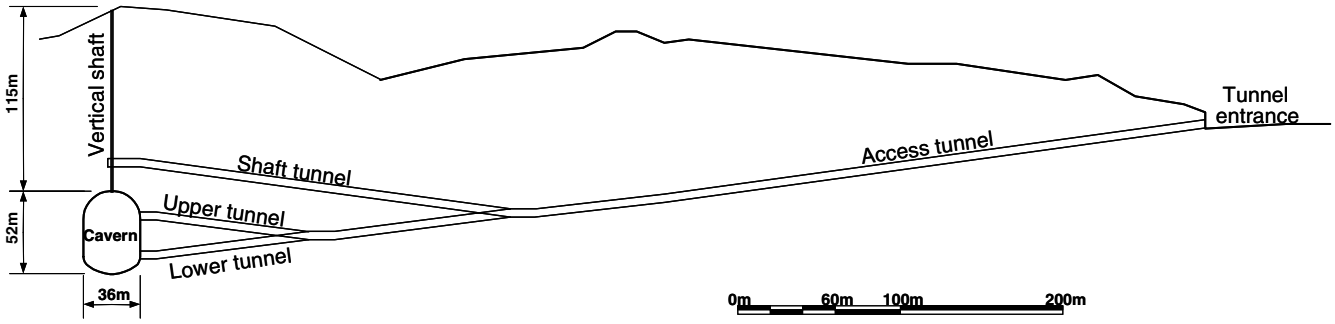

Fig. 2. Layout of storage cavern and access tunnels at the LRC Demo Plant (after Johansson, 2003).

RQD values of 20–40%. Four such dikes were identified during the investigation stage, with thicknesses varying between 1 and 15 m. The cavern position was shifted slightly to avoid them, however, they were encountered in the tunnels, see Fig. 3. An additional thin amphibolite dyke, not identified during the investigation stage, was encountered during the excavation of the cavern itself with an approximate N–S strike and a dip of around 30°E, see Fig. 4. The thickness of the dike is approximately 0.5–0.7 m. The contacts between the dike and the gneiss include some clay filling. The orientation of the dike coincides with the direction of the gneiss foliation. Although additional rock support was required along this section no serious problems were experienced.

The dominating joint sets in the area are NS/20–60W, NS/90, EW/90 and N20–70E/50–70E. In Fig. 5, a joint rose diagram is presented compiled from the measured strike of about 400 joint planes in the cavern. Most fractures are coated with non-softening minerals such as calcite, chlorite and epidote. However, clay mineral coatings occur in fractures within and bordering the dikes of amphibolite.

Rock mass classification has been carried out continuously during excavation, primarily using the Q-index, although the RMR^{89}-system also has been utilised (Barton et al., 1974; Bieniawski, 1989). The evaluated RMR^{89}-value and Q-index are presented in Table 1. The Q-index for the gneiss is greater than 10, corresponding to good rock quality, while the Q-index for the dike of amphibolite encountered in the cavern generally varied between 1 and 4, corresponding to rock of poor quality. Consequently, within the cavern the rock mass is classified as good rock with a dike of poor to locally very poor rock.

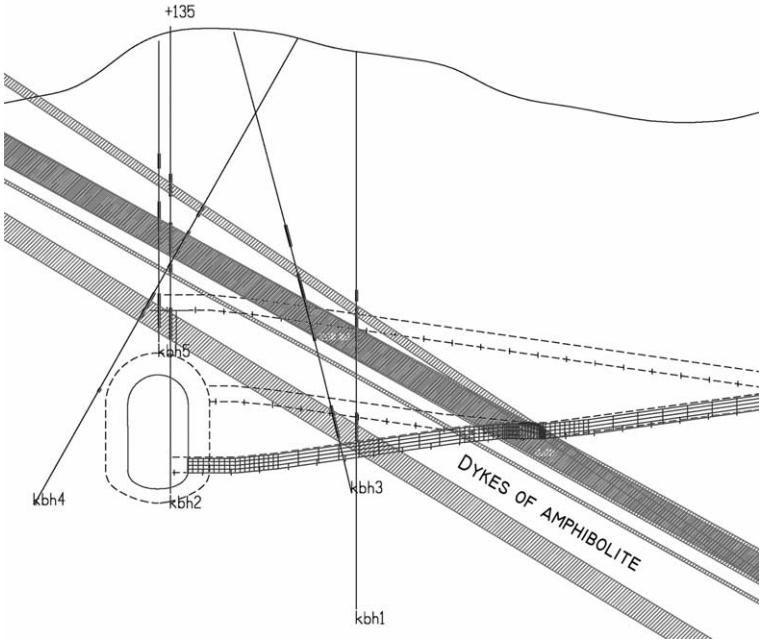

Fig. 3. Geological model of the site in west–east direction there the amphibolite dikes are shaded. The model is interpreted from five core drillholes and mapping along the access tunnels.

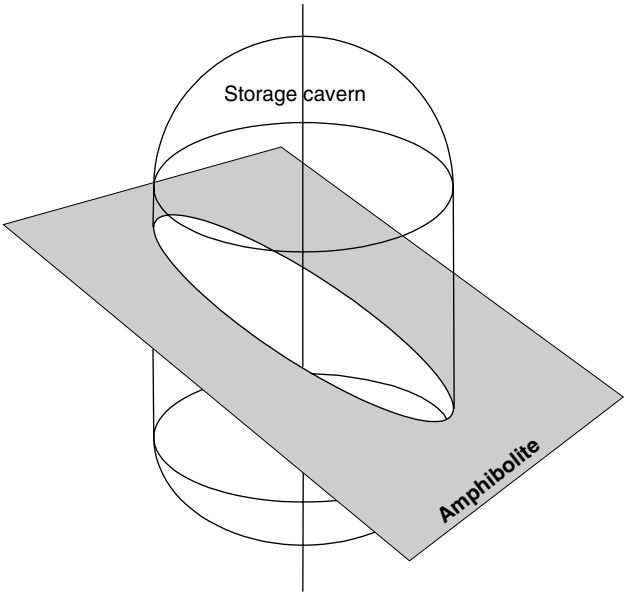

Fig. 4. Location of the Amphibolite dike encountered within the cavern.

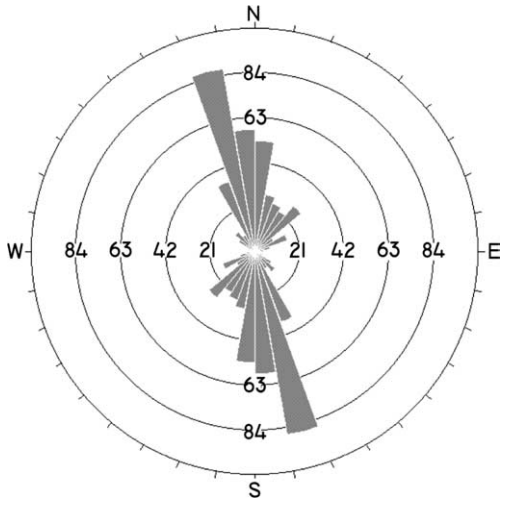

Fig. 5. Joint rose diagram showing the strike of the dominating joints sets based of approximately 400 joint planes mapped in the cavern.

Table 1
Results from the rock mass classification (cavern)

Rock type	RMR89	Q-index	Description
Gneiss	72–86	13–32	Good rock
Amph'	41–60	0.9–4	Poor rock

2.3. In situ stresses

In situ stress measurements were performed in the body of rock where the cavern was to be located. The stress field was determined by overcoring of 4 stress cells and hydraulic fracturing at 13 locations within the depth interval 60–200 m. The evaluated magnitude of the in situ stresses versus depth is presented in Table 2. Rock stress measurements conducted in the area, show in situ stresses slightly under the mean magnitude compiled for the Fennoscandia shield. The vertical stress was assumed to correspond to the theoretical lithostatic stress.

Table 2
Evaluated magnitude of the in situ stress field within the depth interval 60–200 m

	Symbol	Value	Unit
Major horizontal stress component	σ_H	0.061z–0.32	MPa
Minor horizontal stress component	σ_h	0.0295z–0.1063	MPa
Vertical stress component	σ_V	0.0265gz	MPa

Table 3
Evaluated mean values of the rock mass properties in the cavern vicinity based on empirical relations related to RMR89 and Q-index

	Symbol	Value	Unit
Young's modulus	E_m	36.0	GPa
Poisson's ratio	υ	0.2	–
Uniaxial compressive strength	σ_{cm}	50.3	MPa
Cohesion	c	13.4	MPa
Angle of internal friction	ϕ	33.9	Deg
Angle of dilatation	ψ	7	Deg
Tensile strength	T_0	0	MPa
Density	ρ	2650	kg/m^3

The direction of the principal stresses was uncertain and fluctuated up to 90° between the overcoring and the hydrofracturing. Results from the overcoring gave an orientation of σ_H in a N–S direction, while hydrofracturing indicated an orientation around N70–80°E. The second orientation is close to the direction of the gneiss foliation and one of the joints sets observed on outcrops in the field.

2.4. Rock mass properties

The rock mass properties were estimated by empirical relationships relating the properties of the rock mass to the classification system RMR and Q, Barton et al. (1980), Bieniawski (1978), Hoek et al. (1995) and Serafim and Pereira (1983). The most important rock mass properties in relation to the LRC concept are the deformation modulus and the compressive strength. The values used for numerical predictions of deformation during the excavation of the cavern are presented in Table 3. The parameters are based on the site investigation and on observations during excavation of the access tunnels.

3. Excavation sequences

All of the underground excavation was carried out using 'standard' drill and blast techniques. However,

the cavern geometry and the tight tolerances on the final excavated rock contour meant that tight control of the blasting work was required and the contractor needed to take a flexible and imaginative approach to the work. The layout of the cavern, including the steps in the excavation sequence, is presented in Fig. 6. The excavation steps are numbered from I to X, starting with the shaft chamber and ending with the bottom of the cavern.

3.1. Excavation of tunnels

In the tunnels, investigative drilling was carried out from the tunnel face. The temporary support consisted of shotcrete and bolts, and grouting took place when the water inflow was above 10 l/min/100 m of tunnel, although very little water inflow was experienced during tunnel construction.

3.2. Excavation of the shaft

After the completion of the shaft tunnel (step I), leading to a position above the cavern crown, the 1 m diameter 90 m long shaft, linking the gas storage cavern with the surface facility, was raise-bored. The pilot hole for the shaft was drilled from the surface down to a level equal to the bottom of the cavern, a total of 160 m. The operation was carried out within 20 days.

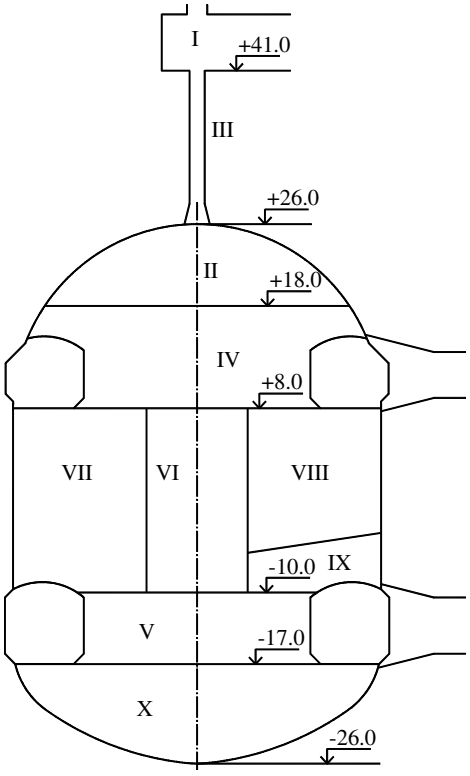

Fig. 6. Vertical section of the cavern showing the steps and levels in the excavation sequence. Ground surface on level +135.

3.3. Excavation of the cavern

From a position inside the upper cavern tunnel entrance (level +8.0), two spiral shaped tunnels were excavated at a steep angle, one up to the left and one to the right, to access the cavern crown (step II), see upper part Fig. 7.

The two tunnels met round the 'back' of the cavern, opposite the initial entrance point. The left spiral was then continued up and over the existing right spiral to level +18.0, see lower part Fig. 7. From this position, it was possible to excavate the cupola in sections installing any necessary temporary support as the work proceeded. This work left approximately 1 m of rock to the theoretical cavern contour. The final contour was achieved by a final stage of careful blasting. Support for the final contour was applied when small sections were opened up 40–70 m^2.

After completion of the roof, the 'floor' of the cupola was sinked in two stages down to level +8.0 (step IV). The contour in this lower part of the cupola was achieved by gross volume blasting followed by careful contour blasting and subsequent rock support.

Drilling of the whole cross-section was carried out (ca. 650 holes) from the level of the upper cavern tunnel (level +8.0). A lower ring tunnel (step V) and a central shaft between the upper and lower tunnel (step VI) were opened for loading and hauling out the rock. Blasting was carried out along the full length of the holes (step VII–VIII). However, a protective 'roof' was left

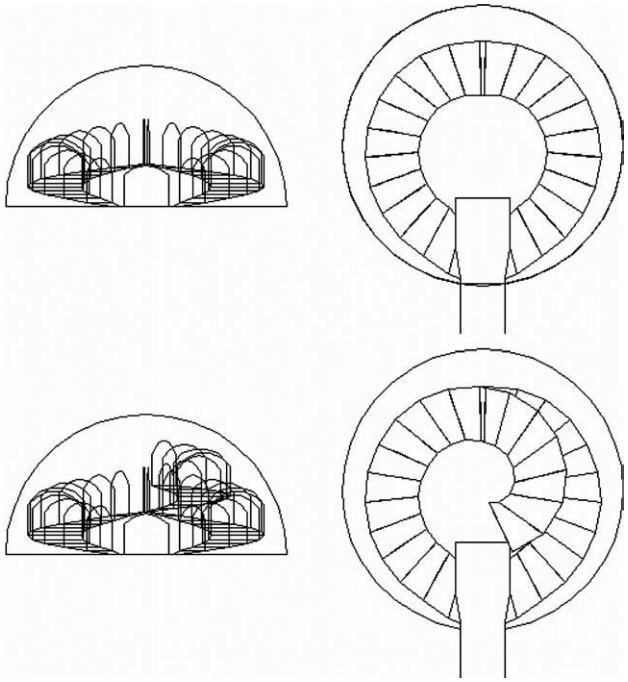

Fig. 7. Schematic illustration of the cavern crown excavation. Upper part showing the spiral tunnels and the bottom part the ramp in the cupola (after Allvin et al., 2001).

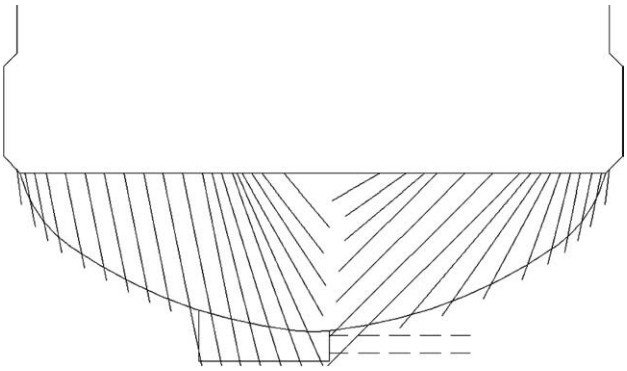

Fig. 8. Vertical section of the cavern bottom showing the drill pattern of the bottom excavation (after Allvin et al., 2001).

(step IX) covering the access to the central shaft position. Mucking was carried out via the central shaft and the two faces of the ring tunnel. Mucking was carried out stepwise, lowering the 'floor' in the cavern, in order to facilitate the installation of the drainage system and permanent support.

The bottom excavation (step X) was carried out using approximately 1000 angled holes laid out in a cone shape focused on the central depression, see Fig. 8.

4. Rock reinforcement

The dimensioning of the rock support in the LRC demo project generally followed the guidelines given in the Q-system (Hoek et al., 1995). However, the recommendations given by the Q-system were reviewed by numerical modelling of the demo plant for the measured in situ stress field. Numerical modelling was also performed to assess the deformation and stress change related to the pressurization of the cavern.

The specified level of support in the cavern, shaft and tunnels was checked by a comparison between the predicted and observed deformation. The support for the cupola consisted of 100 mm fibre-reinforced shotcrete and systematic bolting. The pattern consisted of fully grouted, 25 mm diameter, 6 m long rock bolts placed at 2.5 m centers.

The entire cavern wall was covered by 30 mm unreinforced shotcrete as the excavation progressed. In addition two sectors, 070°–120° and 250°–300°, were supported by 50 mm of fibre-reinforced shotcrete and systematic bolting. The bolts were 4 m in length and spaced on 3 m centers. The bolts were placed to prevent potentially large 'slab failures' in the walls associated with the dominant north–south vertical joint set. In general it can be said that this level of support was conservative when compared with the rock mass quality. However, there was concern with the large size of the potential failures and also the fact that as the cavern floor was lowered it would become increasingly difficult, and costly, to gain access to the upper walls and cupola to carryout any necessary remedial works.

5. Calculated rock mass response

5.1. Model conditions

The rock mass response was calculated by the numerical code FLAC, which is based on the finite difference method (ITASCA, 2000). Two element grids were utilised in the numerical calculation, see Fig. 9. The first grid, model LRC10, represents a quarter of a horizontal plane at the cavern upper niche and the second grid, model LRC20 and LRC30, an axi-symmetric vertical section of the cavern. The reason for using two element grids is that the combination of the in situ stress anisotropy and the cavern geometry with a short axis, cannot be studied satisfactorily in a single 2D model.

The width and height of the horizontal plane were 175×175 m and the width and height of the vertical grid were $W = 125$ m and $H = 250$ m, respectively. The bottom boundary of the vertical grid was located at level −115.0 and the ground surface +135.0. The cavern height is 52.5 m and the cavern radius 18.5 m. The cavern bottom is located −26.5 and the cavern roof at +25.9.

The in situ stress conditions adopted in the models are given in Table 2. The material properties used in the models are listed in Table 3. The Mohr–Coulomb failure criterion has been used with a tension cut-off at 0 MPa, i.e., assuming no tensile strength.

Calculated stresses at some levels in the models are presented in Table 4. Since anisotropy occurs in the horizontal stress field, the complete stress field was studied in two separate axi-symmetric models, LRC20 and

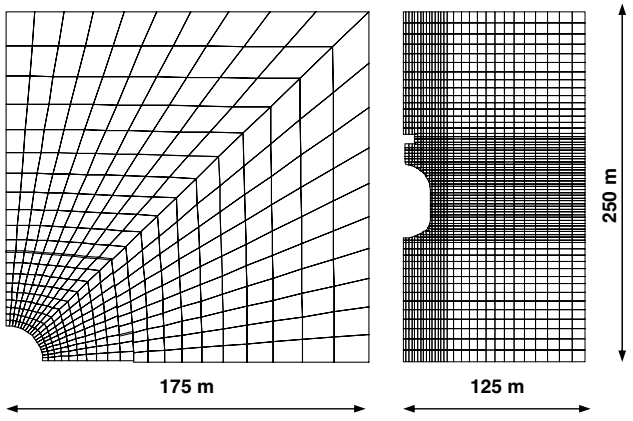

Fig. 9. The element grids used in the numerical calculation. To the left is shown the horizontal plane at the cavern upper niche (LRC10) and to the right the axi-symmetric vertical section of the cavern (LRC20 & 30).

Table 4
Calculated stresses at some levels in the models

Depth (m)	Level	σ_H (MPa)	σ_h (MPa)	σ_v (MPa)
0.0	+135.0	−0.32	−0.11	0.00
109.1	+25.9	6.34	3.11	2.84
124.5	+10.5	7.27	3.57	3.24
135.0	0.0	7.91	3.88	3.51
161.5	−26.5	9.53	4.66	4.20
250.0	−115.0	14.93	7.27	6.50

LRC30. The stress states possible to analyse in an axi-symmetric model are biaxial, i.e., the horizontal stresses in the model are the same in all directions. In the horizontal plane, model LRC10, the in situ stress field was assigned the values evaluated at the upper niche, level +10.5.

The boundary conditions assumed in the models are given in Table 5. The horizontal plane, model LRC10, has a pressure applied in the normal direction on the outer boundaries and the symmetry boundaries are fixed in the normal direction. The axi-symmetrical section, model LRC20 and LRC30, has the ground surface free with an applied pressure in the horizontal direction on the outer vertical boundary, and the two other boundaries are fixed in the normal direction.

The steps in the modelling path, along with the corresponding excavation steps, are given in Table 6. The roman numerals given in the table refer to Fig. 6.

Table 5
Boundary conditions

Model	Boundary	Conditions
LRC10	Outer boundaries	Applied pressure in normal direction
	Symmetry boundaries	Fix in normal direction
LRC20 & 30	Ground surface	Free
	Bottom boundary	Fixed in vertical direction
	Vertical boundary	Applied pressure in horizontal direction
	Axis of symmetry	Fixed in horizontal direction

5.2. Cavern convergence

The computed convergence at the monitoring levels in the cavern cupola is presented in Tables 7–9. The convergence values presented for the horizontal plane correspond to 55% of the calculated convergence. This reduction follows the work by Hanafy (1980), which is necessary since the model LRC10 simulates the cavern as an infinite cylinder, see Appendix.

The largest convergence was calculated in the direction of the major horizontal in situ stress after complete excavation of the cavern. The calculated results in the horizontal plane located at the upper niche, model LRC10, correspond to a convergence of 6.2 mm in north–south direction and 0.8 mm in east–west direction. The axi-symmetrical section, model LRC20 & 30, suggests a convergence of 1.3 mm in the north–south direction and 0.65 mm in east–west direction in the roof, and 3.85 mm in north–south direction and 2.0 mm in east–west direction in the upper niche. The ratio between the maximum and minimum convergence in the final excavation step is 7.75 in the horizontal plane, while only 2 in the axi-symmetric section.

Table 7
Model LRC10, calculated convergences in the upper niche (+10.5)

Excavation step	Reading no.	Convergence, σ_H (mm)	Convergence, σ_h (mm)
IV	1	0.00	0.00
X	5	6.20[a]	0.80[a]

[a] The values correspond to 55% of the calculated convergence according to Hanafy (1980), Appendix.

Table 8
Model LRC20 & 30, calculated convergences in the roof (+24.4)

Excavation step	Reading no.	Convergence, σ_H (mm)	Convergence, σ_h (mm)
III	1	0.00	0.00
IV	2	0.79	0.41
VIII	3	1.16	0.60
IX	4	1.25	0.64
X	5	1.29	0.66

Table 6
Steps in the modelling path

Model	Excavation step	Comments
LRC10	–	Setting of initial conditions in the model
	X	Excavation of the cavern bottom, −16 to −26.5
LRC20 & 30	–	Setting of initial conditions in the model
	I	Excavation of the shaft chamber, level +47.5 to +41
	II	Excavation of the cupola, level +26 to +18
	III	Excavation of the shaft, level +41 to +26
	IV	Excavation of the cavern cupola, level +18 to +8
	V	Excavation of the cavern bottom, level −10 to −16
	VI–IX	Excavation of the cavern cylinder, level +8 to −10
	X	Excavation of the cavern bottom, −16 to −26.5

Table 9
Model LRC20 & 30, calculated convergences in the upper niche (+10.5)

Excavation step	Reading no.	Convergence, σ_H (mm)	Convergence, σ_h (mm)
IV	1	0.00	0.00
VIII	2	3.15	1.65
IX	3	3.67	1.88
X	4	3.86	1.97

Table 10
Model LRC20, calculated deformation in a vertical direction in the cavern roof

Excavation step	Distance 0–8 m (mm)	Distance 0–12 m (mm)	Distance 0–14 m (mm)
II	0.058	0.157	0.281
III	0.042	0.117	0.225
IV	0.010	0.060	0.173
V	0.010	0.060	0.175
VI	0.002	0.045	0.163
VII–VIII	0.002	0.045	0.163
IX	0.000	0.043	0.162
X	0.000	0.042	0.162

Starting point at level +41.0. Positive values corresponds to extension.

5.3. Rock mass deformation

The calculated deformation in a vertical direction in the cavern roof within 0–14 m from the shaft tunnel is presented in Table 10. The computed magnitude amounts to approximately 0.3 mm at excavation of the cavern cupola (step II). During the following excavation steps the deformation decreases to approximately 0.15 mm.

6. Recorded rock mass response

6.1. Monitoring program

The monitoring program during the excavation of the cavern included convergence measurements and extensometer measurements to monitor the stability and deformation of the cupola. The extensometer measurements were carried out automatically using a datalogger whilst the convergence measurements were carried out manually. The results of the numerical analyses carried out during the design, formed the basis for determining where the deformations should be measured. The positions for the convergence measurements and the extensometers installed around the cavern cupola are shown in Fig. 10.

6.2. Cavern convergence

The convergence measurements were performed with the following purpose: (1) to confirm the direction of the principal stress field; (2) to provide a basis for assessing the accuracy of the parameters assigned during the analysis of the cavern stability; (3) control of the stability during excavation.

The convergence measurements in the cavern comprised one roof level location (+24.4) and one level located in a niche (+10.5) between the dome and cylinder, see Fig. 10. The measurement in the roof included optical readings between ten prisms on a radius of 7.5 m with a total station. The convergence measurements in the niche included triangulated measurements between eight anchors on a radius of 19 m. The instrument used in this case was an ISETH distometer. According to the instrument manufacturer the accuracy of the measurements is $\pm 1 \times 10^{-6}$ of the distance; giving a value of 0.04 mm for readings across the cavern. The instrument proved to be both accurate and reliable with repetitive readings within 0.02 mm.

Readings were taken six times in the roof and four times in the niche during a period of half a year as the excavation proceeded in the cavern. The zero reading was taken after excavation step III (May-2000) in the roof and after excavation step IV (July-2000) in the niche. The final readings for both levels were made after completion of excavation step X (November–December-2000), see Fig. 6.

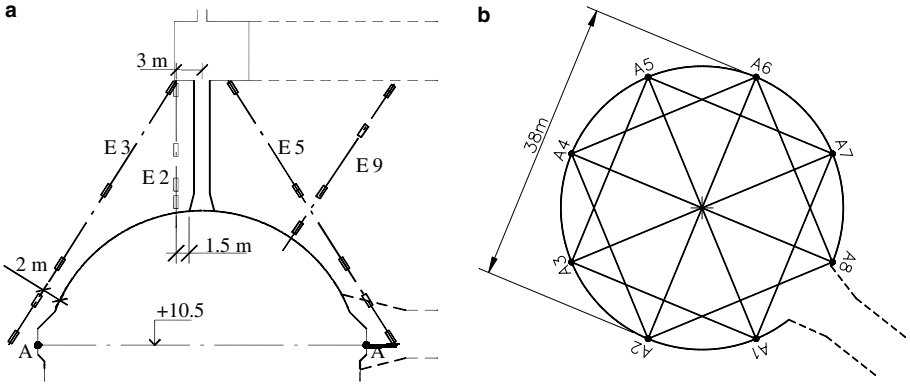

Fig. 10. Positioning of convergence measurements in the cavern (series A) and extensometers around the cupola (series E).

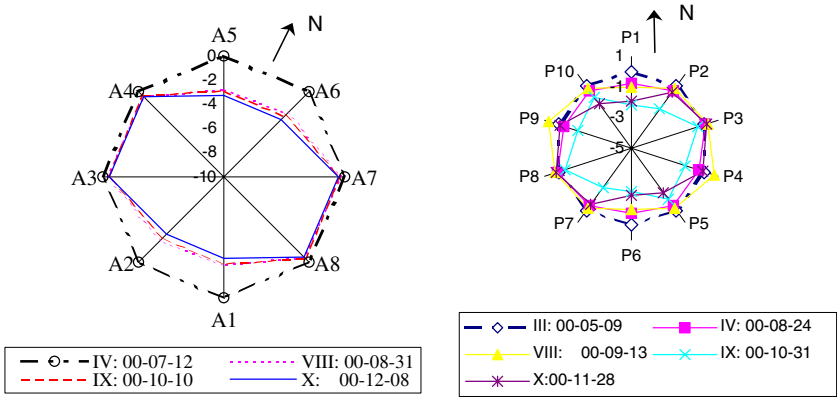

Fig. 11. Recorded cavern convergence during the excavation. To the left is shown convergence in the upper niche and to the right convergence in the cavern roof. The units are in mm.

The results are presented in Fig. 11. The recorded convergence indicates great anisotropy in the deformation field around the cavern. The largest convergence was recorded in sections close to a north–south direction, with approximately 4.0 mm in the roof and about 6.5 mm in the niche. In sections close to an east–west direction, the recorded convergence was around 0.5 mm in the roof and approximately 1.0 mm in the niche. The ratio between the maximum and minimum convergence was approximately 8 in the roof and 6.5 in the niche. Several sections in the roof indicated a decline in the convergence during the final excavation step.

The convergence measurements in the upper niche do not indicate any slip associated with the amphibolite dike. On the contrary the deformation in its dip direction is smaller than the calculated elastic deformation.

It should be noted that the recorded convergence is only a part of the total convergence that took place during the cavern excavation. From a study performed by Hanafy (1980), it is judged that approximately 40% of the deformation took place before convergence readings were initiated in the upper niche.

6.3. Rock mass deformation

A number of extensometers were installed in the rock mass surrounding the storage chamber, see Fig. 10. The extensometers had 3–5 measurement levels and vibrating wire type sensors. Extensometers E2 to E6 and E9 were installed after the excavation of the cavern shaft chamber (excavation step I) in order to monitor the stability and deformation of the cupola during the cavern excavation. However, installation of the instruments was somewhat delayed and excavation of the cupola had progressed somewhat before the taking of readings commenced. This may have led to some of the deformation being missed before the readings were started.

The recorded deformation for extensometer E2, installed in vertical direction above the cavern, is presented in Fig. 12. E2 shows small deformations, there the magnitude amounted to 0.6 mm at the shaft excavation (step III). During the following excavation steps the deformation decreased down to around 0.2 mm. The result corresponds to a slight rise of the cavern roof as the excavation of the cavern progressed downwards.

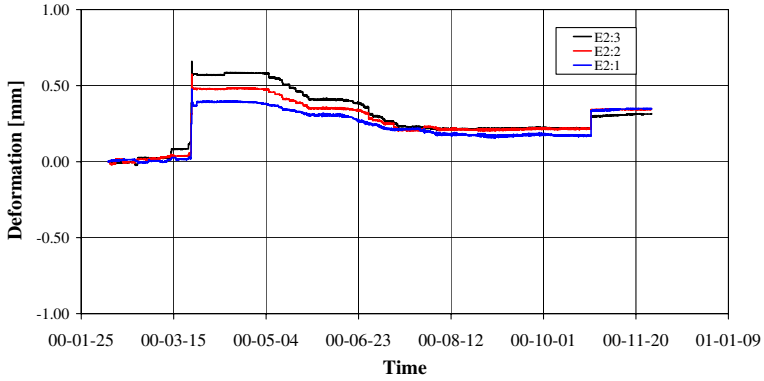

Fig. 12. Recorded deformation along extensometer E2. Positive deformation corresponds to extension. The units are in mm.

The deformation across the amphibolite dike above the cupola has been very low. E9 installed in a radial direction to the cavern cupola has not shown any significant deformation associated with the amphibolite. The recorded deformation has been in level with the numerical calculated deformation with the dike omitted.

7. Comparison between calculated and recorded deformations

The recorded convergence is in good agreement with the values evaluated from the results in the horizontal model simulating a plane located at the upper niche. The difference being only about 5% in the north–south direction and 20% in the east–west direction. The recorded ratio between major and minor convergences is also in close agreement with the calculated ratio in the model.

The agreement is, however, considerably poorer between recorded and calculated convergence in the axi-symmetric model. The recorded convergence in the north–south direction in the niche is approximately 1.7 times higher than the calculated value. In the east–west direction the opposite case occurs, with the calculated convergence being twice the recorded value. The conditions are similar in the roof level. However, the divergence between recorded and calculated deformation is higher in the north–south direction and lower in east–west direction. The recorded ratio between major and minor convergences is also several times higher than the calculated ratio.

In the direction of extensometer E2 in the cavern roof, the recorded and calculated deformations show a similar deformation trend as the excavation progressed. However, the recorded deformation magnitude is 0.3 mm larger than the calculated and amounts to approximately twice the calculated value in excavation step II and III.

8. Discussion

The divergence between the recorded and calculated deformation varies considerably between the two models that have been used. The results show that a true evaluation of the observed cavern behaviour ought to be performed in a three-dimensional model. The combination of in situ stress anisotropy, cavern geometry and excavation procedure is difficult to describe correctly without simulation in a three-dimensional model. However, comparison between the recorded and calculated convergence in the upper niche indicates that the greatest credence should be given to the results in the horizontal plane after reduction for the limited extent of the cavern axis, see Appendix.

Table 11
Results from parameter study of the in situ stress ratio in horizontal direction assuming an isotropic rock mass modulus

σ_H (MPa)	σ_h (MPa)	k	Xd[a] (mm)	Yd[b] (mm)	Ratio
7.27	1.82	4.0	0.98	−6.40	−6.53
7.27	2.42	3.0	0.38	−6.09	−16.03
7.27	2.91	2.5	−0.09	−5.88	65.33
7.27	3.57	2.0	−0.73	−5.64	7.73
7.27	3.83	1.9	−0.98	−5.68	5.79
7.27	4.04	1.8	−1.18	−5.46	4.63
7.27	4.85	1.5	−1.95	−5.16	2.65

[a] Displacements in X-direction.
[b] Displacements in Y-direction.

Table 12
Results from parameter study of the rock mass modulus assuming an in situ stress ratio of 2

E_x (GPa)	E_y (GPa)	G (GPa)	Xd[a] (mm)	Yd[b] (mm)	Ratio
18	36	10.6	−1.64	−6.52	3.97
26	36	12.9	−1.05	−6.03	5.74
28	36	13.4	−0.96	−5.93	6.18
30	36	13.8	−0.89	−5.86	6.58
32	36	14.3	−0.82	−5.76	7.02
36	36	15.0	−0.73	−5.64	7.73

[a] Displacements in X-direction.
[b] Displacements in Y-direction.

Special importance was placed on the recorded ratio between the major and minor convergence during the evaluation of the results. In the axi-symmetric model the ratio is in direct proportion to the assumed in situ stress anisotropy. The horizontal model on the other hand shows a much larger convergence ratio, which is similar to what has been observed in the cavern. This result is important since it clearly demonstrates that it is mainly the in situ stress field that is causing the observed anisotropy in the cavern convergence. This fact is not clear from the results in the axi-symmetric model.

The recorded and calculated convergence are in opposite directions with reference to the minor direction if an in situ stress ratio greater than 2.5 is assumed in the model. This condition supports the assumption that the anisotropy in the in situ stress field is in the right range. In the case of an isotropic rock mass modulus the evaluated difference corresponds to an in situ stress ratio of 1.95, see Table 11, while in the case of an in situ stress ratio of 2 the difference corresponds to a ratio 1.2 in the rock mass modulus, see Table 12.

9. Conclusions

The experience from the project shows that the stability of a large silo shaped cavern can be achieved with only light rock support when the rock mass is of good

quality. The cavern excavation was carried out without any major rock engineering problems. Only one large block fall-out occurred in the cupola close to the shaft. The outfall occurred along clay-filled sub-horizontal joints.

The decision to locate the cavern below and beyond amphibolite dikes to avoid any weakness zone in the cupola proved to be a good decision since it avoided potential stability problems and wedge failures interfering with the production of a satisfactory final contour to the cavern surface. Only a small amphibolite dike crossed the main body of the cavern and this did not cause any stability problems after sealing with fibre-reinforced shotcrete. However, the zone was a source of repeated minor problems during the blasting work. During the excavation of the cavern (step VII) repeated minor wedge failures along planar joints, parallel to the amphibolite's dip direction, disrupted a number of blast holes.

The recorded convergence confirms the stress field evaluated from the overcoring technique. The largest convergence was recorded in sections close to a north–south direction, with approximately 4.0 mm in the roof and around 6.5 mm in the niche. The ratio between the maximum and minimum convergence was approximately 8 in the roof and 6.5 in the niche. The results are in good agreement with the convergence predicted by the model simulating a horizontal plane at the upper niche.

The recorded deformation in the vertical direction in extensometer E2 amounted to 0.6 mm, while the calculated deformation is approximately 0.3 mm. The recorded deformation is thus about twice the calculated, which could be considered as rather high if corresponding to the same difference in rock mass modulus. However, the difference in absolute values is small and could be an effect of a single fracture opening due to gravitational forces or of uncertainty in the measurements.

Acknowledgements

The authors acknowledge LRC Demo AB for permitting the publishing of data from the design and construction phase of the LRC Demo Plant.

Appendix. Displacements associated with a tunnel face advance

Distance between the monitoring level (+10.5) and the face in excavation step IV (level +8)

$(10.5 + 8)/18.5 = \mathbf{0.14R} \rightarrow \mathbf{0.38}$.

Distance between the faces in excavation step IV (level +8) to X (level −26)

$(8 - (-26))/18.5 = \mathbf{1.84R} \rightarrow \mathbf{0.93}$

→The recorded convergence comprises only 55% of the convergence calculated in a horizontal plane in the level of monitoring (+10.5) (see Fig. A1).

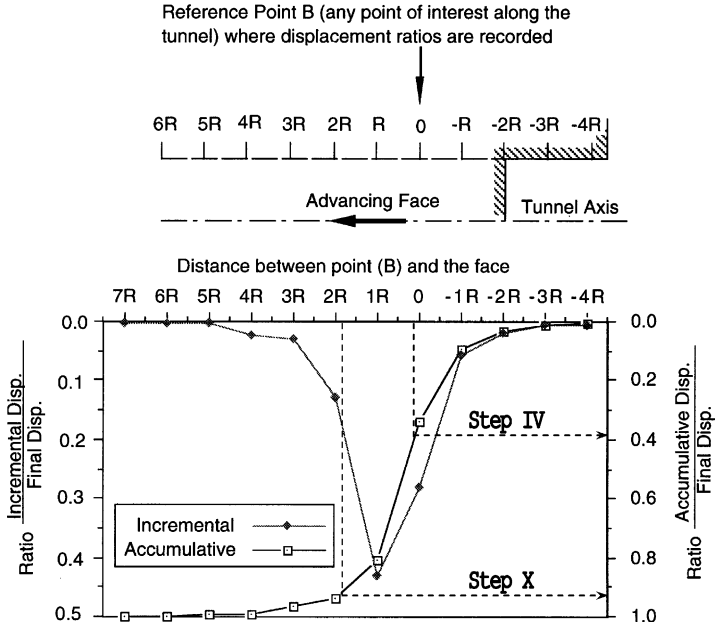

Fig. A1. Radial displacement of a reference point (B) associated with tunnel face advance for an unlined tunnel under elastic conditions (modified after Hanafy, 1980).

References

Allvin, C., Sturk, R., Tengborg, P., 2001. Advanced Rock Excavation of a Lined Gas Storage, LRC Demo, Getinge. In: Proceedings of BK-Conference, Stockholm, pp. 79–91 (in Swedish).

Barton, N., Løset, F., Lien, R., Lunde, J., 1980. Application of the Q-system in design decisions. Sub Surface Space, vol. 2. Pergamon, New York, pp. 553–561.

Barton, N., Lien, R., Lunde, J., 1974. Engineering classification of rock masses for the design of tunnel support. Rock Mech. 6 (4), 189–239, Springer-Verlag.

Bieniawski, Z.T., 1989. Engineering Rock Mass Classifications. Wiley, New York.

Bieniawski, Z.T., 1978. Determining rock mass deformability – experience from case histories. Int. J. Rock Mech. Min. Sci. & Geomech. Abstr. 15, 237–247.

Hanafy, E.A., 1980. Advancing face simulation of tunnel excavation and lining. Placement. In: Underground Rock Engineering, 13th Canadian Rock Mechanics Symposium, pp. 119–125.

Hoek, E., Kaiser, P.K., Bawden, W.F., 1995. Support of Underground Excavations in Hard Rock. A.A. Balkema, Rotterdam.

ITASCA Consulting Group, Inc., 2000. User's Manual, Minneapolis.

Johansson, J., 2003. High Pressure Storage of Gas in Lined Rock Caverns – Cavern Wall Design Principles. Licentiate Thesis. Div. of Soil and Rock Mech., Royal Institute of Technology, Stockholm.

Serafim, J.L., Pereira, J.P., 1983. Consideration of the geomechanical classification of bieniawski. In: Proceedings of International Symposium on Engineering Geology and Underground Construction, Lisbon, vol. 1 (II), pp. 33–44.